Effect of the oxidation state of gold on the complete oxidation of isobutane on Au/CeO_2 catalysts

Fang Ying[a], Shuiju Wang[b], Chak-Tong Au[a] and Suk-Yin Lai[a,*]

www.goldbulletin.org

Abstract

Catalysts of highly dispersed gold supported on ceria were prepared by deposition precipitation method. Au is dispersed as Au^0, Au^+ and Au^{3+} species on ceria. The content of Au^+ and Au^{3+} was highest on catalyst prepared on uncalcined ceria, which possess least ordered surface. It is inferred that oxygen vacancy on disordered ceria surface is essential for the preparation of highly dispersed gold catalysts and in stabilizing monolayer surface Au^+ clusters while cationic vacancies are sites for substitutional Au^{3+}. Au/CeO_2 catalysts showed low-temperature isobutane oxidation activity with maximum conversion at 150-180°C. Ex-situ XPS results demonstrated that the low temperature isobutane oxidation activity was closely related to the content of Au^+ which we interpreted as surface gold oxide formed under reaction conditions. Isobutane oxidation activity associated with ceria at temperature above 300°C was enhanced by substitutional Au^{3+}.

[a] *Department of Chemistry and Centre for Surface Analysis and Research, Hong Kong Baptist University, Kowloon Tong, Hong Kong, China*
[b] *State Key Laboratory for Physical Chemistry of Solid Surface, Xiamen University, Xiamen, 361005, China*

* *Corresponding author*
E-mail: laisy@hkbu.edu.hk

1 Introduction

Au/CeO_2 catalysts have been found to exhibit high activity in various reactions, one of the most intensively studied is the complete oxidation of volatile organic compounds (VOCs) (1-8). The catalytic activity depends mainly on the morphology of ceria particles, gold particle size and the oxidation state of gold species. In general, nanosize gold particles with diameter less than 5 nm supported on nanocrystalline CeO_2 have been demonstrated for high activity in VOCs oxidation reactions (1, 5, 6).

Despite numerous studies, the nature of the gold species in active VOCs oxidation catalysts is still under debate. The participation of cationic gold in reactions over gold catalysts has been discussed quite widely (7-10). Shen et al. found that Au/CeO_2 catalyst with highly dispersed metallic gold and small amount of oxidized gold exhibited superior catalytic activity for HCHO oxidation (7). Likewise, Liu et al. reported that Au/CeO_2 calcined at 300°C exhibited high content of cationic gold species and excellent activity for 2-propanol complete oxidation (8). The results stimulated much study on the nature of gold on ceria, both experimentally and theoretically and have provided important insight into the interaction between gold and ceria. Based on results of density functional theory calculation, Liu et al. deduced that O vacancies act as anchoring sites for Au, and a Au atom adsorbed on an O vacancy is negatively charged and is inactive in binding CO. Other gold atoms bound to this kind of anchored atoms, forming a monolayer gold cluster, are positively charged through electron transfer to the f orbitals of cerium (11). The more recent DFT+U calculation of Camelone and Fabris also predicted that Au atoms on O vacancies to be negatively charged while Au atom supported on stoichiometric $CeO_2(111)$ to be Au^+. These authors also deduced that Au atoms substituted for cerium in the $CeO_2(111)$ lattices

have charge corresponding to the Au^{3+} state. The substitutional gold ions cause distortion of the surrounding lattices and are highly active for CO oxidation (12). Experimentally, partial reduction of cerium from Ce^{4+} to Ce^{3+} by deposition of gold on CeO_2(111) was demonstrated by Skoda et al. using resonant photoelectron spectroscopy (13). Using STM and RAIRS of CO adsorption on gold, Naya et al. showed that positively charged gold was formed when gold was deposited on CeO_2(111) surfaced with oxygen vacancies while gold deposited on the stoichiometric surface is uncharged (14). In a different study on the interaction of atomic oxygen with Au(111) using DFT calculation, Shi and Stampfl predicted that a surface gold oxide phase should be stable up to 420 K at atmospheric pressure of oxygen. They suggested that surface gold oxide can play a significant role in the catalysis by gold (15).

The present study focused on the preparation of Au/CeO_2 with high fraction of cationic gold species by the deposition-precipitation method and the identification of the active centers in the complete oxidation of light alkanes, using isobutane as a test compound.

2 Experimental

Nanocrystalline CeO_2 was prepared by first dissolving 5 g $Ce(NO_3)_3 \cdot 6H_2O$ in 100 mL D.I. H_2O under ultrasonication, then 0.005 g/mL NaOH aqueous solution was added gradually with vigorous stirring during the ultrasonication until the pH value was 10. The mixture became a light purple colloid. After 1 h further ultrasonication, the precipitate was centrifuged out and the recovered CeO_2 was washed three times with D.I. water. The obtained product was divided into three portions. One portion was simply dried at 100°C whereas the others were calcined in air at 300 or 500°C for 4 h. The samples are denoted hereinafter as CeO_2-100, CeO_2-300 and CeO_2-500 respectively.

Gold was loaded onto the CeO_2 samples by deposition-precipitation by stirring ceria powders in a solution of chloroauric acid in deionized water at pH 10 for 5 h at room temperature. Then the suspension was filtered out and washed several times with D.I. water. Finally, the obtained sample was dried at 100°C for 12 h and calcined at 300°C for 4 h. The so-obtained catalysts are denoted as Au/CeO_2-100, Au/CeO_2-300 and Au/CeO_2-500.

X-ray diffraction (XRD) analysis was conducted on a Rigaku D-MAX diffractometer with Ni-filtered Cu Kα radiation. N_2 adsorption-desorption isotherms were recorded on a Quantachrome NOVA-1200 instrument. ICP-AES using a Perkin-Elmer Optima 3000 spectrometer was applied to determine the gold content of the catalysts. The catalyst surface compositions were determined by X-ray photoelectron spectroscopy (XPS) over a Leybold Heraeus-Shengyang SKL-12 electron spectrometer equipped with a VG CLAM 4 MCD electron energy analyzer, using Al-Kα as excitation source. High-resolution transmission electron microscopy (HRTEM) investigation was performed on a JEOL TEM-2100 operating at 200 kV.

H_2-temperature programmed reduction (H_2-TPR) was performed in a flow reaction system using a 5% H_2 in N_2 mixture with flow rate of 50 mL min^{-1}. Hydrogen consumption was monitored by a Gow-Mac thermal conductivity detector with prior removal of water vapor by means of a liquid-N_2 cold trap. The samples were oxidized in a flow of synthetic air with flow rate 25 mL min^{-1} at 300°C for 60 min before TPR experiment. Quantity of hydrogen consumption and hence degree of reduction of ceria after reduction to different temperature was determined by calibration with the reduction of a known amount of CuO. With the CeO_2-100 sample, an additional run on a fresh sample without pre-oxidation at 300°C, denoted as CeO_2-100*, was performed. The reduction behavior of this sample is considered more representative of the surface property of CeO_2-100 support used for the preparation of Au/CeO_2-100.

Isobutane oxidation was carried out in a fixed-bed flow reactor at atmospheric pressure. In each run, 0.2 g of catalyst (80-40 mesh) was loaded in a quartz tubular reactor (8-mm i.d.) and activated in synthetic air at 300°C for 2 h before reaction. Then 1% isobutane in synthetic air at a flow rate of 50 mL/min was passed over the catalyst at designated temperature, and the products were analyzed on-line with a Shimadzu 8A gas chromatograph with a methanizer and flame ionization detector.

3 Results and discussion

3.1 Morphological and textural characterization

The specific surface area of the CeO_2 samples decreased only slightly from 88 to 72 m^2 g^{-1} with increasing calcination temperatures from 100 to 500°C. Addition of gold did not change the catalyst surface area significantly.

Figure 1

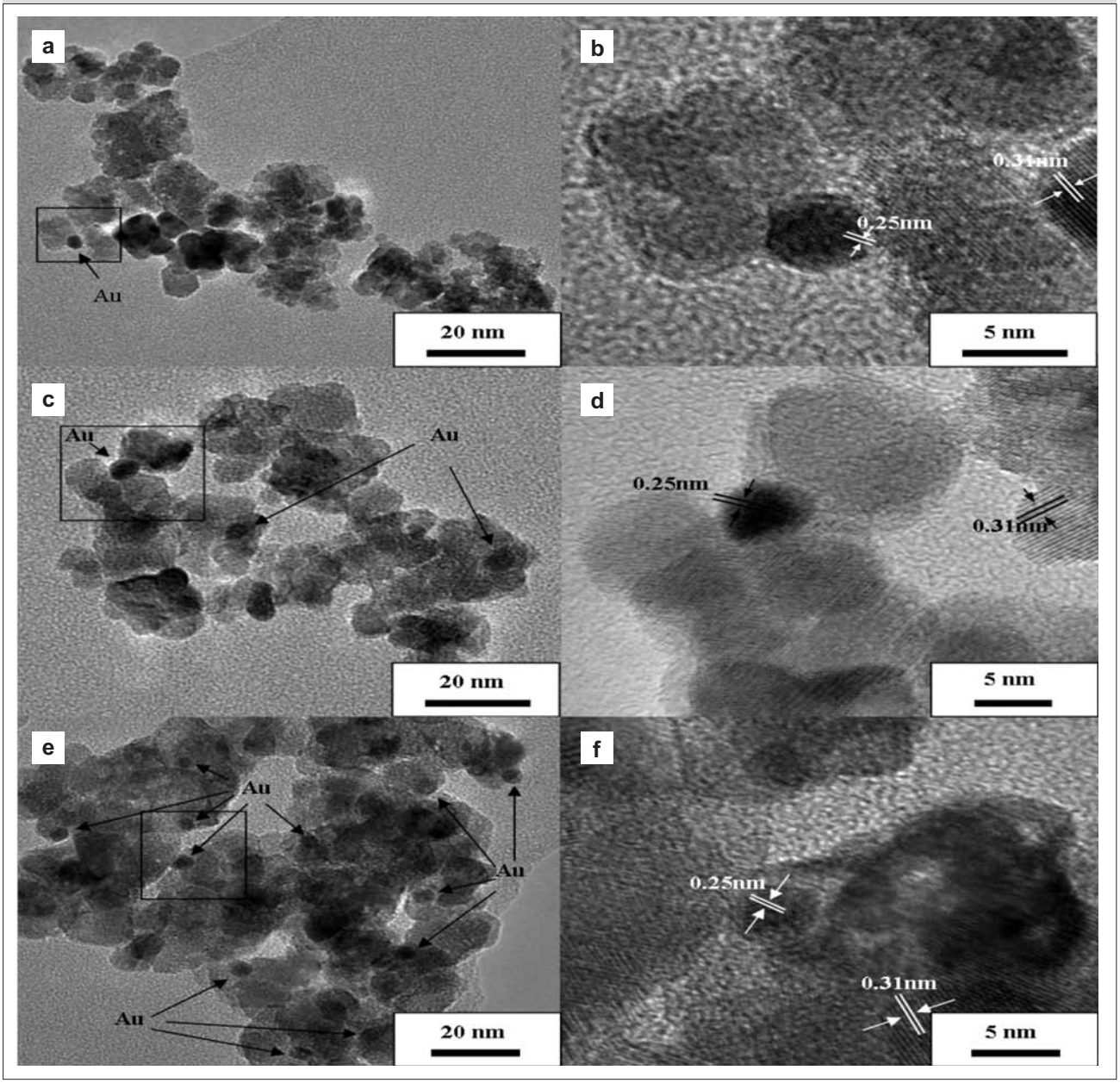

HRTEM of different Au-containing catalysts: (a,b) Au/CeO_2-100; (c,d) Au/CeO_2-300; (e,f) Au/CeO_2-500

The mean size of crystalline CeO_2, calculated from the broadening of the (111) X-ray diffraction line using the Scherrer equation, was in the narrow range of 10.6 to 12.2 nm, suggesting that sintering was not significant up to 500°C, in agreement with the surface area data. X-ray diffraction peaks attributable to gold could hardly be detected over any of the gold-loaded samples showing that gold was highly dispersed. The gold loading of all the Au/CeO_2 catalysts obtained from ICP-AES results were in a narrow range of 1.7-1.9 wt%.

Representative HRTEM images of Au/CeO_2 are shown in Figure 1. Figures 1(a), 1(c) and 1(e) are images at nominal magnifications from ×100,000 to ×200,000 showing the general features of the samples. Selected areas of the sample indicated were studied in higher magnification and shown in Figures 1(b), 1(d) and 1(f) to show the crystal lattice fringes. Au/CeO_2-100, Au/CeO_2-300 and Au/CeO_2-500 contained discrete crystalline CeO_2 particles with the size of 10 to12 nm in agreement with the XRD results. Although the CeO_2 samples were

Table 1: XPS results of catalysts

Catalyst	Surface composition			Position of Au $4f_{7/2}$ peak	Au species distribution[a]		
	Au (mol%)	Ce (mol%)	O (mol%)	Binding Energy (eV)	Au^0 (%)	Au^+ (%)	Au^{3+} (%)
CeO_2-100	-	22.1	77.9	-		-	-
CeO_2-300	-	26.6	73.4	-		-	-
CeO_2-500	-	27.1	72.9	-		-	-
Au/CeO_2-100	0.5	28.4	71.1	84.6	13.0	50.1	36.9
Au/CeO_2-300	0.4	28.6	71.0	83.8	60.7	18.6	20.7
Au/CeO_2-500	0.5	28.6	70.9	83.6	71.8	15.8	12.4

[a]: The measured XPS peak area for the Au species as a percentage of the total gold peak area

calcined at different temperatures, no significant difference in CeO_2 particle size and morphologies was found among the three samples.

Gold particles with lattice spacing of 0.25 nm can be detected in all the three gold-containing samples. It should be pointed out that gold particles with a diameter of ca. 4 nm were only occasionally detected in Au/CeO_2-100. Most dark particles such as the one shown at the right edge of figure 1(b) turned out to be nanocrystalline ceria particles. Despite the scarcity of identified gold particles, about 2% by weight of gold was found in the region in Figure 1(a) by EDS, indicating that gold was indeed present at the expected concentration, probably in the form of clusters that were too small to be observed or even atomically dispersed. Many more gold particles with an average diameter of 3-5 nm were found dispersed throughout the other two samples, especially for Au/CeO_2-500.

3.2 Surface chemical state

The surface concentration of Au, Ce and O and the distribution of the different Au species are summarized in Table 1. The Au 4f spectra of the catalysts, with binding energy corrected for charging effect using the 917 eV Ce u''' peak as internal binding energy reference, are shown in Figure 2. The binding energies of Au $4f_{7/2}$ were 84.6 eV, 83.8 eV and 83.6 eV for Au/CeO_2-100, Au/CeO_2-300 and Au/CeO_2-500 respectively. The binding energy difference shows that the chemical state of Au is affected by the nature of the ceria support. To quantify the difference, the Au 4f spectra were

Figure 2

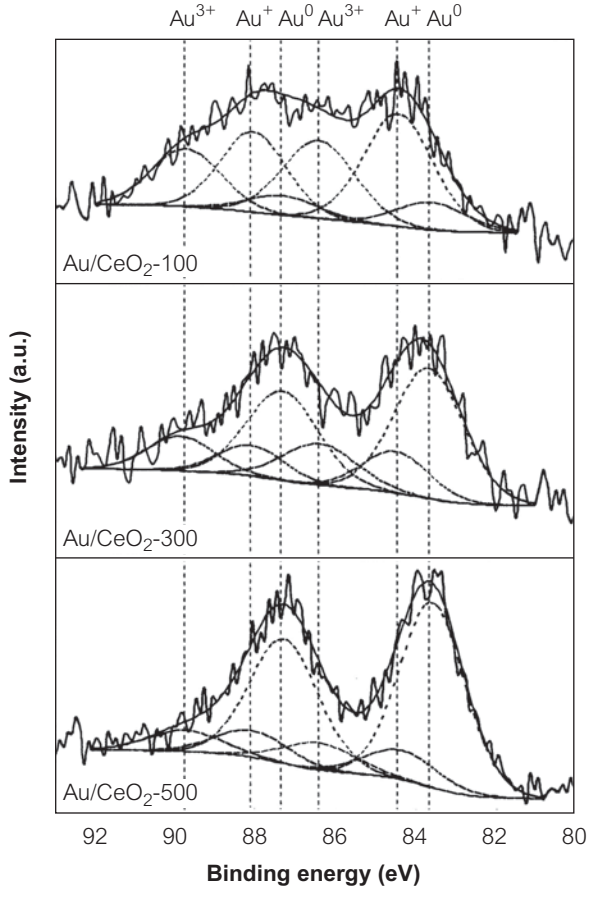

XPS profiles of Au 4f region for Au/CeO_2 samples

resolved into 3 doublets corresponding to Au^0 ($4f_{7/2}$ B.E. at 83.6 eV), Au^+ ($4f_{7/2}$ B.E. at 84.4 eV) and Au^{3+} ($4f_{7/2}$ B.E. at 86.4 eV).

Cationic gold species were dominant in Au/CeO_2-100 while mainly metallic gold was found in Au/CeO_2-300 and Au/CeO_2-500. As listed in Table 1, the fraction of metallic gold increased with the rise in calcination temperature of CeO_2. Based on the HRTEM and XPS results, we suggested that gold mainly existed as highly dispersed cationic species on the surfaces of CeO_2-100, whereas metallic gold particles were the main gold species in Au/CeO_2-500. Since the same deposition-precipitation condition was adopted, the appearance of different gold species among the three samples must originate from the different thermal treatment of the CeO_2 support.

3.3 Temperature programmed hydrogen reduction

The redox behaviors of the CeO_2 materials and gold-containing samples were studied by H_2-TPR and the results are shown in Figures 3 and 4. Two sets of peaks representing the reduction of surface-capping oxygen and bulk phase lattice oxygen were found for CeO_2 materials (16). The reduction peak temperature

Figure 3

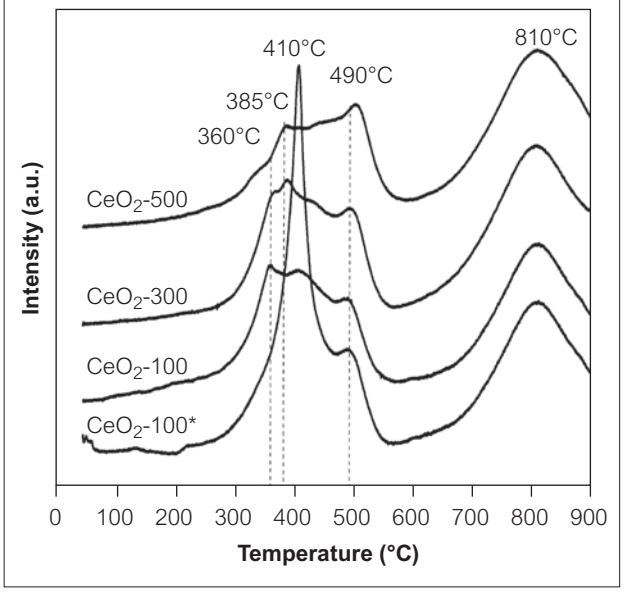

H_2-TPR profiles of CeO_2 catalysts (CeO_2-100: sample without pre-oxidation at 300°C in air before TPR experiment)*

Figure 4

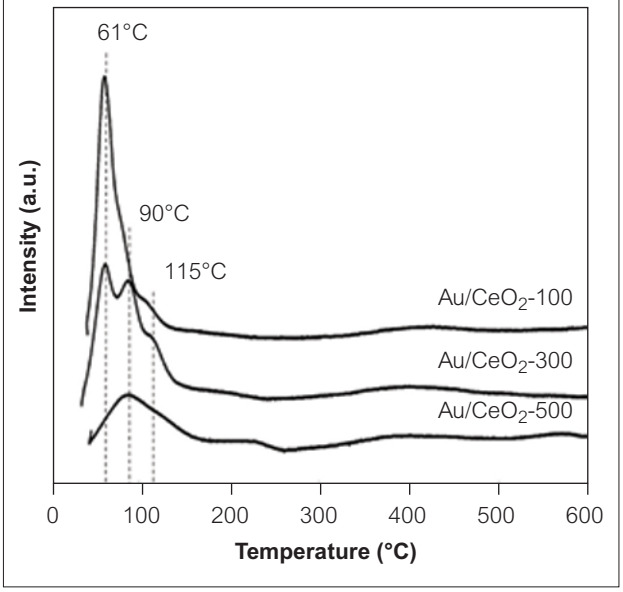

H_2-TPR profiles of gold-containing samples

Table 2: H_2-TPR results of different samples

Catalyst	Peak temperature (°C)	H_2 consumption for surface oxygen reduction up to 550°C ($\mu mol/g_{cat}$)	"x" in CeO_x after H_2 reduction to 550°C
CeO_2-100*	300-550	794	1.86
CeO_2-300	300-550	742	1.87
CeO_2-500	300-550	683	1.88
Au/CeO_2-100	61-107, 500	1169 (977[a])	1.80
Au/CeO_2-300	62-140, 500	1247 (1029[a])	1.80
Au/CeO_2-500	62-210, 500	951 (569[a])	1.84

CeO_2-100*: catalyst without pre-oxidation at 300°C in air before TPR experiment
a: H_2 consumption up to 250 °C

and corresponding hydrogen consumption for the surface reduction peaks below 550°C are listed in Table 2. With the gold-containing samples the amount of H_2 consumption at temperature below 250°C are given in brackets.

CeO_2-100* gave two reduction peaks at 410°C and 490°C. The TPR profiles of CeO_2-100, CeO_2-300 and CeO_2-500 are quite different. As all three samples had undergone pre-oxidation in air at 300°C for 1h, they should be considered as samples after calcination at increasing severity. The most significant differences of the calcined samples compared to CeO_2-100* are (i) the increase in prominence of the 490°C peak, which also shifted to a higher peak temperature around 500°C on increasing calcination severity, (ii) the reduction in intensity of the 410°C peak, and (iii) the concomitant appearance of peaks at 360 and 385°C. Reduction of ceria surface at around 500°C was well documented in the literature, especially for well-calcined nanocrystalline ceria (17, 18). It is well known that the (111) plane is thermodynamically the most stable (19). With calcination, well defined facets bound by stable low-index planes is expected to develop and (111) facets eventually would become the most prominent exposed surface. Hence we attribute the 500°C peak to reduction of (111) surfaces. The 360 and 385°C peaks were attributed to corners and edges at the boundary of the crystallite facets. The broad feature in between we attribute to reduction of the less stable (110) and (100) facets of the crystallites. As CeO_2-100* was not calcined, its surface should be more disordered and contained more defects. Hence, we ascribe the peak at 410°C to the reduction of poorly crystalline ceria surfaces.

With the addition of Au, the main part of the low-temperature reduction peak shifted to the much lower temperature of 60-120°C. Since the amount of H_2 required to reduce $Au^{\delta+} \rightarrow Au^0$ over these catalysts is less then 140 μmol/g, much less than the H_2 consumed below 250°C, we ascribe the low temperature reduction peaks to the reduction of gold-activated ceria surface. For Au/CeO_2-100, a main reduction peak at 61°C with two shoulder peaks at about 82°C and 115°C were observed, whereas two peaks of similar height at 61°C and 90°C with a relatively weaker peak at 115°C were found for Au/CeO_2-300. Au/CeO_2-500 showed only one broad peak in the 50-140°C range. It is known that metallic gold in analogy with other noble metals may activate hydrogen that spillover to nearby ceria, thus promoting the reduction of ceria at lower temperature (20). For highly dispersed Au/CeO_2, reduction peak at 60-180°C had been reported, with lower reduction temperature indicating stronger interaction between gold and the support (19, 21-23). In our experiment, the existence of three reduction peaks might indicate that the different gold species identified by XPS activate surface oxygen for reduction in slightly different manners.

Data in Table 2 show that the H_2 consumption for Au-containing samples was higher than that for pure CeO_2 by amount more than that required to reduce ionic gold, suggesting that some sub-surface ceria was reduced after the addition of gold.

3.4 Catalytic activity

The catalytic activity of CeO_2 and Au/CeO_2 for isobutane oxidation is shown in Figure 5. Carbon dioxide and water were the only detected products and carbon mass balance was higher that 95%. Isobutane oxidation activity over the gold-free samples is similar. This could be understood since all samples were activated by air at 300°C for 2h before the reaction and TPR data showed that the surfaces were rather similar after such activation.

Gold enhanced the isobutane oxidation activity significantly. At 350°C, while the isobutane conversion over all three CeO_2 supports was

Figure 5

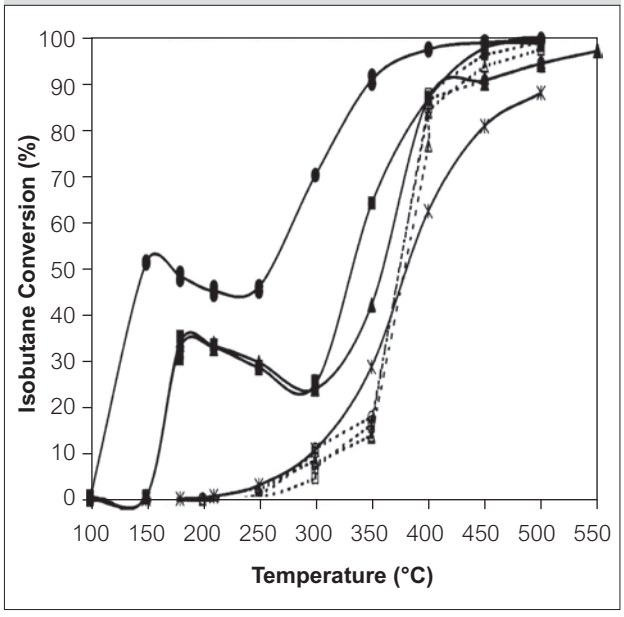

(a) Activity for isobutane oxidation over different catalysts. (●) Au/CeO_2-100; (■) Au/CeO_2-300; (▲) Au/CeO_2-500; (○) CeO_2-100; (□) CeO_2-300; (△) CeO_2-500; (✱) reference Au/TiO_2 distributed by the World Gold Council

Table 3: Surface composition of the catalysts after reaction under different conditions

Catalyst	Surface composition				Position of Au $4f_{7/2}$ peak	Au species distribution		
	Au (mol%)	Ce (mol%)	O (mol%)	Au/Ce	Binding Energy (eV)	Au^0 (%)	Au^+ (%)	Au^{3+} (%)
Au/CeO_2-100	0.45	28.2	71.3	0.016	84.6	13.0	50.1	36.9
Au/CeO_2-100(180)	0.37	31.6	68.1	0.012	84.0	54.0	32.6	13.4
Au/CeO_2-100(280)	0.31	29.9	69.8	0.010	83.8	72.4	14.2	13.4
Au/CeO_2-100(500)	0.16	23.8	76.1	0.007	83.6	75.8	1.4	22.8
Au/CeO_2-100(500-180)	0.25	28.7	71.1	0.009	83.7	68.9	10.5	20.6
Au/CeO_2-100(500-30)	0.26	32.8	67.0	0.008	83.9	46.0	24.6	29.4
Au/CeO_2-100(180)*	0.21	27.0	72.8	0.008	83.7	64.9	13.5	21.6

Au/CeO_2-100(180): catalyst was treated at 180°C under reaction condition for 1h, then cooled down in N_2 to room temperature.

Au/CeO_2-100(500-180): catalyst was first used in isobutane oxidation at temperature from 200-500°C, then cooled down to 180°C in the reactant stream and maintained at 180°C for 1h before finally cooled down to room temperature in N_2.

Au/CeO_2-100(180)*: catalyst after stability test at 180°C, cooled down in N_2 to room temperature.

Figure 6

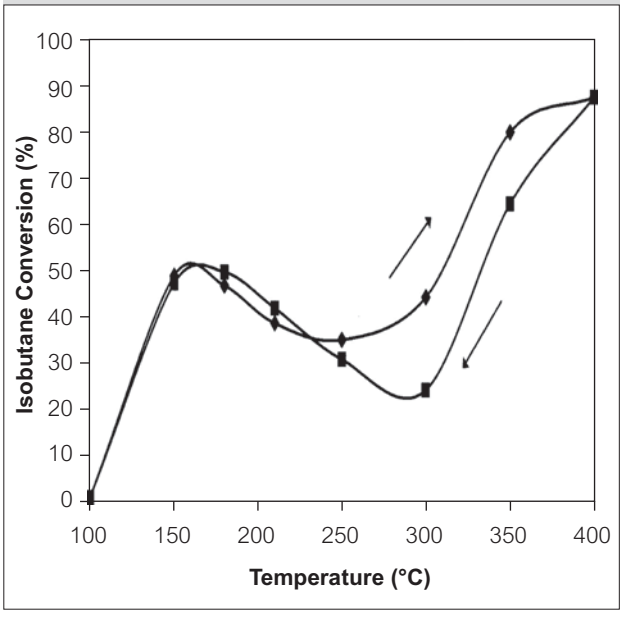

Catalytic activity of Au/CeO_2-100 determined when the reaction temperature was increased (◆) and decreased (■) in the reactant stream

between 10-20%, the conversion over Au/CeO_2-500, Au/CeO_2-300 and Au/CeO_2-100 were increased to 42%, 64% and 91% respectively. More interestingly, for the Au-containing catalysts, an additional low-temperature volcano-shaped activity profile was found. Isobutane conversion increased with increasing reaction temperature up to 150-180°C; the activity then declined with increasing temperature between 180 and 300°C. Further increase of temperature resulted in rise in isobutane conversion again. For comparison, we carried out the isobutane oxidation reaction over the A-type reference Au/TiO_2 catalyst supplied by the World Gold Council. The reference Au/TiO_2 showed isobutane oxidation activity similar to that of the ceria supports; the low-temperature activity was completely absent. The reference catalyst has highly dispersed gold and very high activity for CO oxidation. Complete oxidation of 1% CO to CO_2 in air was found in our laboratory at room temperature. Hence, we infer that having highly dispersed gold is not a sufficient condition for low temperature isobutane oxidation activity. Our Au/CeO_2 catalysts all contain some cationic gold, and Au/CeO_2-100, the catalyst showing the highest low temperature activity, possesses the highest proportion of cationic gold. Thus, it is logical to ascribe the isobutane oxidation activity to cationic gold species.

To examine the temperature effect more thoroughly, we studied the isobutane activity of a fresh sample

Figure 7

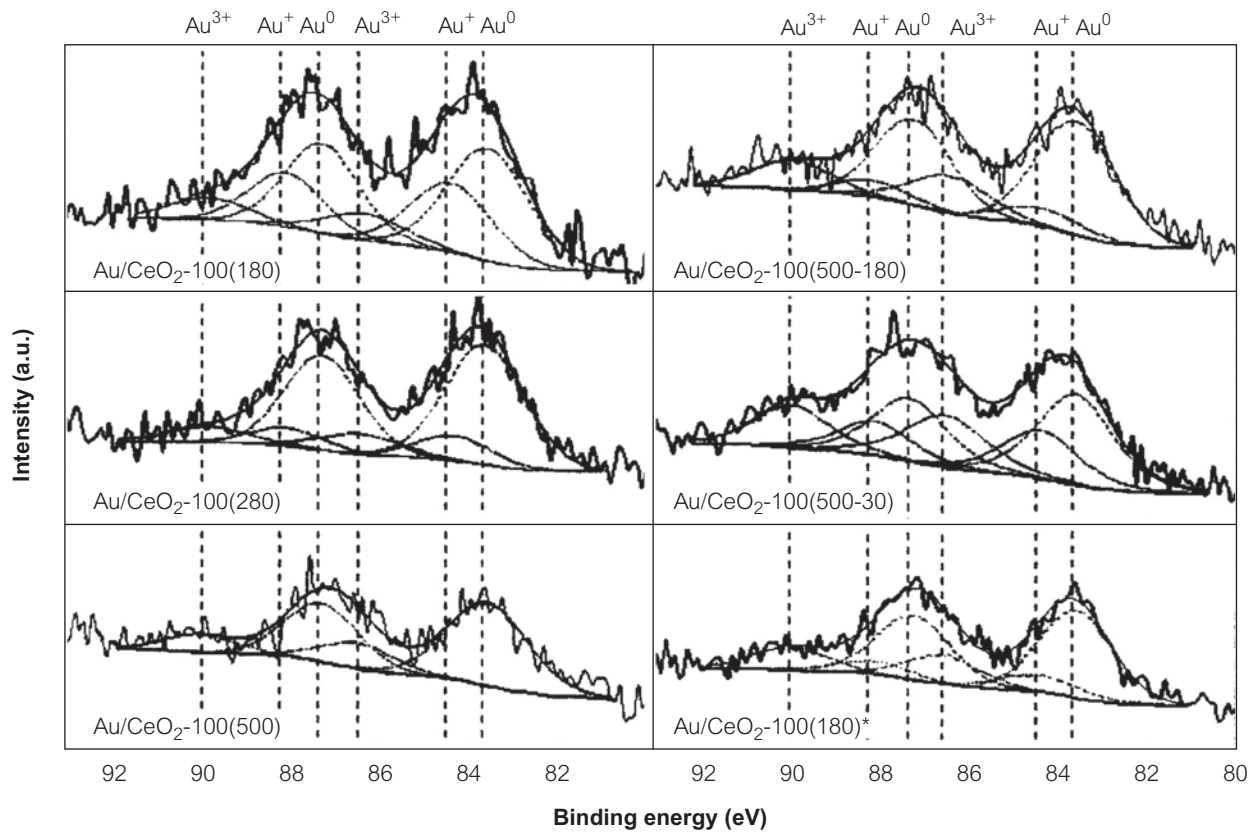

XPS profiles of Au 4f region on Au/CeO_2-100 after various treatments. Au/CeO_2(T): the sample was treated in the reactant stream at T°C for 1h, then cooled in N_2 to room temperature before analysis by XPS; Au/CeO_2(500-T): After exposure to the reactant at 500°C, the sample was cooled down to T°C in reactant gas and finally cooled in N_2 to room temperature before analysis by XPS. Au/CeO_2-100(180): catalyst after stability test at 180°C, cool down in N_2 to room temperature*

of the most active catalyst, Au/CeO_2-100 with the temperature of the catalyst bed raised stepwise from 100°C to 400°C. Without reactivation, the temperature of the catalyst bed was then lowered to 100°C stepwise while the activity was monitored. The result in Figure 6 showed that a hysteresis loop of activity versus temperature appeared at temperature higher than 250°C, suggesting that the catalyst was deactivated. However, when the temperature fell below 250°C, the low-temperature conversion was recovered. From this observation, we infer that self poisoning by the accumulation of strongly adsorbing reaction products such as surface carbonate is not the cause of the catalyst deactivation between 150 and 250°C since desorption of such species leading to reactivation could not happen when the catalyst bed temperature was lowered. Furthermore, a sample of the catalysts was subjected to prolonged reaction at 180°C. Isobutane conversion increased slightly from 50% to around 55% in the first five hours and then maintained more or less constant in the next 90 hours. The absence of catalyst deactivation at constant temperature further ruled out poisoning by adsorbed reaction products. Reversible change in the chemical nature of the catalyst surface is a more probable reason for the peculiar behavior of the catalysts for isobutane oxidation.

3.5 The importance of cationic gold in isobutane oxidation reactions

Activity hysteresis loop was also observed by Zhang et al. on $AuO_x/Ce_{0.6}Zr_{0.3}Y_{0.1}O_2$ catalysts in methane oxidation (24). They suggested that the hysteresis loop was caused by the partial reduction of the more active AuO_x to less active Au^0 as well as the Ce^{4+} in CZY to Ce^{3+} at high temperature. Similarly, for methane oxidation over Pd, deactivation at high temperature due to decomposition of the more active Pd-O and reactivation at low temperature by reoxidation of Pd was known (25).

With this background in mind, we performed ex-situ XPS measurement of the catalysts surface in an attempt to elucidate how the surface chemical state of the catalyst changes during the reaction.

Samples of Au/CeO_2-100 were exposed to the reaction gas mixture at different temperatures for about 35 min. To preserve the surface condition, the samples were cooled to room temperature in a stream of nitrogen before XPS analysis. We denote these samples as Au/CeO_2-100(T) where T is the temperature of exposure in °C of the catalyst to the reactant gas. To study the reversibility of the oxidation state change, two catalyst samples were first heated to 500°C and then cooled in the reactant gas to 180°C and 30°C before switching to nitrogen flow. These samples were denoted as Au/CeO_2-100(500-180) and Au/CeO_2-100(500-30). The catalyst after prolonged reaction at 180°C for 100 h was also analyzed and denoted as Au/CeO_2-100(180)*. The XPS analysis results are summarized in Table 3 and the Au 4f spectra are shown in Figure 7. The fraction of gold in the metallic state increased with temperature increase from 180 to 280°C under the reaction condition. There is a correlation between the cationic gold content and isobutane oxidation activity - the activity decreased along with the gold reduction. After carefully examining the XPS data, we found that the change of Au^+ and Au^{3+} are quite different. When the reaction temperature changed from 180 to 280°C, the concentration of Au^{3+} was almost unchanged while Au^+ was diminished by almost 56%. After reaction at 500°C, Au^+ species could hardly be detected. On the catalysts that were cooled in the reactant gas after 500°C treatment, a partial recovery of the Au^+ concentration with decreasing temperature was observed although the degree of gold oxidation over the fresh catalyst was never recovered. On the other hand, the variation of Au^{3+} with temperature was more irregular. While reaction at 500°C nearly completely eliminated Au^+ from the catalyst surface, significant amount of Au^{3+} remained. From the observation, we deduced that the low-temperature activity is associated with Au^+ whereas the enhancement of the catalytic activity above 300°C is associated with Au^{3+}.

3.6 Origin of the active sites for isobutane oxidation

We have associated low-temperature isobutane oxidation activity to Au^+ species. The Au-CeO_2-100, prepared from uncalcined CeO_2-100, was revealed by H_2-TPR to have disordered surface. This same sample contains a much higher fraction of Au^+ and Au^{3+} compared to those supported on the CeO_2-300 and CeO_2-500 with better crystallinity. We infer that both Ce and O vacancies exist at high concentration over CeO_2-100 and the former acts as sites for trapping substitutional Au^{3+} while the latter stabilizing small monolayer Au^+ clusters.

Reduction of such Au^+ species to Au^0 during reaction at increasing temperature should be accompanied by transformation of monolayer Au clusters into thicker multilayer Au particles. Data shown in Table 3 revealed that surface concentration of Au was highest on the fresh Au/CeO_2-100 sample. The surface Au/Ce ratio dropped significantly from 0.016 on the fresh catalyst to 0.007 on the catalyst after reaction at 500°C, suggesting that an increase in the thickness of the Au clusters had indeed occurred. However, on cooling the catalyst from 500°C to 30°C, the regeneration of the Au^+ species was not accompanied by redispersion of Au. The surface Au/Ce ratio remained in the 0.007 to 0.009 range. If the Au particles remained in the multilayer structure, then conversion of Au^0 to Au^+ has to be attributed to oxidation of the multilayer Au clusters. On closer examination of the surface chemical characteristic of Au/CeO_2-100(180) and Au/CeO_2-100(180)*, we note that with increasing time of reaction from 1 hour to 100 hours, the surface Au/Ce ratio decreased from 0.012 to 0.008, and the fraction of Au^+ decreased from 32.6% to 13.5%. During the first 5h of reaction at this temperature, the conversion of isobutane showed a slight increase, in apparent contradiction to our deduction that Au^+ is the active species for oxidation of butanes. This suggested that rather than the initially present positively charged monolayer Au clusters, surface gold oxide that formed during the reaction is the active species. That low-temperature isobutane oxidation observed on Au/CeO_2 but not on the reference Au/TiO_2 catalyst highlights the role of CeO_2. We propose that ceria adjacent to the very small gold particles supplies reactive oxygen to gold for isobutane oxidation as well as maintaining the gold surface oxidized.

At high temperature, oxidation of hydrocarbon over transition metal oxide is often assumed to involve the participation of lattice oxygen (26-29). We suggest that above 300°C, the promotion effect of gold is due to substitutional Au^{3+} reducing the Ce-O bond strength and hence increasing the rate of butane oxidation.

Conclusions

Results of this work suggest that uncalcined high surface area ceria possesses high concentration of both cationic and anionic vacancies that stabilized substitutional Au^{3+} ions and positively charged monolayer gold clusters. Substitutional Au^{3+} ions weaken the Ce-O bond, facilitating the oxidation of isobutane above 300°C. Monolayer Au clusters were converted into small multilayer gold particles during isobutane oxidation. With a supply of active oxygen from the adjacent ceria support, formation of surface gold oxide provides additional active sites for low-temperature oxidation of butane not available over the pure ceria support. The most active catalyst in this study gave isobutane conversion about 55% at the very low temperature of 180°C. The catalyst showed no sign of deactivation for isobutane oxidation over a period of 100 h.

Acknowledgement

This work is supported by a Faculty Research Grant from the Hong Kong Baptist University (FRG1/08-09/061).

About the authors

Ying Fang got his master's degree in Physical Chemistry (2007) at the Xiamen University with researches in the field of heterogeneous catalysis. Ying joined Dr. Lai's research group at the Hong Kong Baptist University in Dec 2006 as a PhD student. His present research focuses on the development, synthesis, and characterization of ceria supported noble metal catalysts for VOCs complete oxidation.

Shuiju Wang is Professor of the State Key Laboratory for Physical Chemistry of Solid Surface at Xiamen University. He is a member of ISO/TC201 (Surface Chemical Analysis). His research interest is in the physical chemistry of solid surface, micro-nanometer scale structural analysis of materials, and in heterogeneous catalysis.

Chak-Tong Au is Professor of Department of Chemistry of the Hong Kong Baptist University. Before joining HKBU in 1990, he did research in the University College, Cardiff, Wales and then joined the Department of Chemistry, Xiamen University in 1986 as associate professor and was promoted to professor in 1987. In 2003, he was awarded D.Sc. degree by the University of Liverpool in recognition of his contributions in the field of surface science and heterogeneous catalysis. At present, he serves as associate editor of the Elsevier journal Applied Catalysis A: General.

Suk-Yin Lai is Associate Professor at the Department of Chemistry and Director of the Centre for Surface Analysis of the Hong Kong Baptist University. Her research interest is in the application of solid catalysts in pollution abatement and in the application of surface analysis techniques for catalyst characterization.

References

1 G.C. Bond, and D.T. Thompson, *Catal. Rev. Sci. Eng.*, 1999, **41**, 319
2 S.-Y. Lai, Y. Qiu, and S. Wang, *J. Catal.*, 2006, **237**, 303
3 D. Andreeva, R. Nedyalkova, L. Ilieva, and M.V. Abrashev, *Appl. Catal. A: General*, 2003, **246**, 29
4 C.D. Pina, N. Dimitratos, E. Falletta, M. Rossi and A. Siani, *Gold Bull.*, 2007, **40**, 1
5 G. Munteanu, L. Ilieva, R. Nedyalkova and D. Andreeva, *Appl. Catal. A: General*, 2004, **277**, 31
6 S. Scire, S. Minico, C. Crisafulli, C. Satriano and A. Pistone, *Appl. Catal. B: Environmental*, 2003, **40**, 43
7 Y. Shen, X. Yang, Y. Wang, Y. Zhang, H. Zhu, L. Gao and M. *Jia, Appl. Catal. B: Environmental*, 2008, **79**, 142
8 S.Y. Liu and S.M. Yang, *Appl. Catal. A: General*, 2008, **334**, 92
9 Q. Fu, H. Saltsburg and M. Flytzani-Stephanopoulos, *Science*, 2003, **301**, 935
10 S. Carrettin, J. Guzman and A. Corma, *Angew Chem, Int Ed*, 2005, **44**, 2242
11 Z.P. Liu, S.J. Jenkins and D.A. King, *Phys. Rev. Lett.*, 2005, **94**, 196102
12 M.F. Camellone and S. Fabris, *J. Am. Chem. Soc.*, 2009, **131**, 10473
13 M. Škoda, M. Cabala, I. Matolinová, K.C. Prince, T. Skála, F. Šutara, K. Veltruská and V. Matolín, *J. Chem. Phys.*, 2009, **130**, 034703

14 K. Naya, R. Ishikawa and K. Fukui, *J. Phys. Chem. C*, 2009, **113**, 10726
15 H. Shi and C. Stampfl, *Phys. Rev. B*, 2007, **76**, 075327
16 H.S. Yao, and Y.F.Y. Yao, *J. Catal.*, 1984, **86**, 254
17 D. Terribile, A. Trovarelli, C. de Leitenburg, G. Dolcetti and J. Llorca, *Chem. Mater.*, 1997, **9**, 2676
18 Y.D. Bi, W. Zhang, H.Y. Xu and W.Z. Li, *Catal. Lett.*, 2007, **119**, 126
19 A.M. Venezia, G. Pantaleo, A. Longo, G. DiCarlo, M.P. Casaletto, F.L. Liotta and G. Deganello, *J. Phys. Chem. B*, 2005, **109**, 2821
20 M. Machida, D. Kurogi and T. Kijima, *J. Phys. Chem. B*, 2002, **107**, 196
21 W. Deng, A.I. Frenkel, R. Si and M. Flytzani-Stephanopoulos, *J. Phys. Chem. C*, 2008, **112**, 12834
22 M. Manzoli, F. Boccuzzi, A. Chiorino, F. Vindigni, W. Deng, and M. Flytzani-Stephanopoulos, *J. Catal.*, 2007, **245**, 308
23 B.E. Solsona, T. Garcia, C. Jones, S.H. Taylor, A.F. Carley and G.J. Hutchings, *Appl. Catal. A: General*, 2006, **312**, 67
24 Y. Zhang, J. Deng, L. Zhang, W. Qiu, H. Dai and H. He, *Catal. Today*, 2008, **139**, 29
25 D. Ciuparu, M. Lyubovsky, E. Altman, L. Pfefferle and A. Datye, *Catal. Rev. – Sci. Eng.*, 2002, **44**, 593
26 S. Minico, S. Scire, C. Crisefulli, R. Maggiore and S. Galvano, *Appl. Catal. B: Environmental*, 2000, **28**, 245
27 S. Zhao and R.J. Gorte, *Appl. Catal. A: General*, 2003, **277**, 129
28 A.C. Gluhoi, N. Bogdanchikova and B.E. Nieuwenhuys, *J. Catal.*, 2005, **229**, 154
29 C. Cellier, V. Ruzux, C. Lahousse, P. Grange and E.M. Gaigneaux, *Catal. Today*, 2006, **117**, 350